APPLICATION OF B3Y-FETAL EFFECTIVE INTERACTION ON CLUSTER RADIOACTIVITY

W.A. Yahya [a,b], J.T. Majekodunmi [c], K.J. Oyewumi [b]
S.A. Bello [b], T.O. Lawal [b]

[a]Department of Physics and Materials Science, Kwara State University
Malete, P.M.B. 1530, Ilorin, Kwara State, Nigeria
[b]Department of Physics, University of Ilorin, Ilorin, Nigeria
[c]Department of Physics, College of Science, Engineering and Technology
University of South Africa
Private Bag X6, Florida 1710, Johannesburg, South Africa

Received 28 September 2025, accepted 1 December 2025,
published online 7 January 2026

In this study, the B3Y-Fetal NN interaction, originating from the lowest order constrained variational approach (LOCV), is applied to investigate cluster radioactivity in energetically favoured trans-lead nuclei from ^{221}Fr to ^{242}Cm within the preformed cluster model, using the Wentzel–Kramers–Brillouin (WKB) theory. Five density-dependent parametrizations are considered to ascertain the most suitable one for cluster radioactivity. The statistical cluster preformation probability is employed and compared with the well-known empirical mass-dependent preformation factor. The predictive power of the BDB3Y1 and BDB3Y0 with the statistical probability is found to give the most accurate description of decay half-lives. These findings underscore the applicability of the B3Y-Fetal interaction in cluster radioactive decays and the reliability of statistical preformation probability in exploring similar decays within the uncharted region of the nuclear landscape. Furthermore, our results demonstrate that DDB3Y1 can aptly address the peculiarity and deviations known for ^{14}C clusters, which is a strongly bound nucleus with $N/Z = 1.33$. The extension of this study to the prediction of energetically favoured but unobserved cluster radioactive decays holds prospects for future experimental endeavours.

DOI:10.5506/APhysPolB.57.1-A3

1. Introduction

Effective interactions are indispensable computational tools for calculations related to finite nuclei and nuclear matter. These interactions are termed "effective" because they are designed to capture the essential features of the complex many-body dynamics in a more practical and computationally manageable way. The development of effective nucleon–nucleon (NN)

interactions is motivated by the limitations of using free NN potentials to describe the behaviour of an atomic nucleus due to the intricate many-body correlations and interactions among its nucleons [1]. Effective NN interactions are constructed by fitting experimental data, such as nuclear masses and radii, to obtain coefficients that describe the strength and range of the interactions. These interactions are particularly advantageous due to their ability to incorporate significant parameters for both symmetric and asymmetric nuclear matter. They are known for their successful description of the properties of nuclei around the β-stability line and exotic nuclei having large neutron or proton excess [2].

One of the most widely adopted effective interactions is the Michigan three Yukawa (M3Y) interaction, which was obtained by fitting the G-matrix elements of Reid [3] and Paris [4] in an oscillator basis. However, various density-dependent upgrades of the original M3Y have been developed [5] to account for higher-order exchange effects, Pauli blocking exchange effects, and to overcome its failure to accurately reproduce the saturation properties of nuclear matter. Similarly, the relativistic three Yukawa (R3Y) NN potential has been derived from the well-known relativistic mean-field (RMF) Lagrangian [6–8] and has been successful in its application to fusion dynamics [9, 10], alpha decay [8, 11–13], and cluster radioactivity [14–17]. In each case, the authors concluded that the R3Y NN interaction, which contains the nonlinear terms, produced a relatively closer alignment with the experimental data. Inspired by the work of Bertsch *et al.* [3], a new effective NN potential titled Botswana three Yukawa (B3Y)-Fetal interaction has been derived from the lowest-order constrained variational (LOCV) principle [18, 19]. Interestingly, the authors demonstrated that the B3Y-Fetal interaction is apt at predicting the nuclear incompressibility $K_0 \approx 176$–235 MeV, which falls within the acceptable range of the experimentally measured data from giant monopole resonances (GMR) wherein, for symmetric nuclear matter (SNM) at equilibrium, nuclear incompressibility $K_0 \approx 240 \pm 20$ MeV [20, 21]. Since cluster decay half-lives are very sensitive to the choice of the effective NN interaction [14, 22], we are spurred to investigate the effect of the new B3Y-Fetal interaction and its various density-dependent forms on cluster radioactivity.

Cluster radioactivity is a decay process that is intermediate between alpha decay and spontaneous fission [23]. This decay process was first predicted by Sandulescu *et al.* [24], and the first experimental evidence was reported by Rose and Jones [25] after they observed the emission of ^{14}C from ^{223}Ra. Subsequently, clusters that are heavier than ^{14}C, such as ^{20}O, ^{23}F, ^{22,24,26}Ne, ^{28,30}Mg, and ^{32,34}Si from some parent nuclei in the trans-lead region, have been experimentally observed [26, 27]. The daughter nuclei are the doubly magic nucleus ^{208}Pb or the neighbouring nuclei such as ^{207}Tl, $^{207,209-212}$Pb, ^{211}Bi, and $^{204-208}$Hg [17, 23, 28–30]. The theoretical models

proposed to study cluster radioactivity can be mainly categorized into two: the fission-like model [31–33] and the preformed cluster model [34–36]. In the fission-like model, it is assumed that the parent nucleus is continuously deformed as it penetrates the nuclear barrier, and the cluster is formed like fission fragments. In the preformed cluster model, the cluster is assumed to be pre-born within the parent nucleus with a particular cluster formation probability. This implies that the latter considers a cluster as an entity that can be pre-formed with a certain probability P_c. However, the parameter P_c cannot be directly measured, and yet its precise value can be very difficult to calculate due to the intricacies of the nuclear many-body problem. Hence, several empirical expressions have been formulated [16, 37–42] that consider the possible influential parameters on P_c. A correlation has been recently obtained between the parameter P_c and the mass number of the preformed cluster within the framework of statistical physics [43]. One of the notable distinctive features of the statistical P_c expression is that it incorporates a dimensionless parameter x, indicating the exact nuclear density at which cluster formation occurs [43].

In view of the discussions above, the present study is geared towards investigating the suitability of the newly developed B3Y-Fetal interaction and its various density-dependent forms on experimentally validated and energetically favoured but unobserved cluster radioactive decay half-lives using the statistical P_c. We reiterate that although similar studies have been carried out, this study extends the literature by considering, for the first time, the applicability of the B3Y-Fetal interaction, which stems from the LOCV principle, on cluster decay. The nuclear interaction within the cluster–daughter system is evaluated by employing the double-folding model [44]. The penetration probability of the cluster is calculated using the semi-classical Wentzel–Kramers–Brillouin (WKB) approximation. Although nuclear deformation is known to impact the preformation probability, this study assumes spherical configurations, the consideration of nuclear deformation will be considered in a future study. Section 2 is dedicated to the framework employed in this study which includes the double-folding model, B3Y-Fetal interaction and its various density-dependent upgrades, conditions imposed in the calculation of the cluster-decay half-lives, and details of the statistical P_c formula. The results are elaborately discussed in Section 3. The inferences drawn from the study are concisely presented in Section 4.

2. Density-dependent cluster model (DDCM)

This study will be carried out using the density-dependent cluster model (DDCM) [45, 46]. Cluster radioactivity involves the doubly magic nucleus, ^{208}Pb, or the neighbouring nuclei, which are spherical or weakly deformed.

Although the importance of considering the deformation of the cluster and daughter nuclei has been stated in Refs. [47, 48], in this study, we take the cluster and daughter nuclei to be spherical. By initially focusing on the spherical assumption, we aim to establish a baseline understanding of the effect of the B3Y-Fetal interaction on cluster radioactivity, which can be extended to other degrees of freedom in future research.

The effective interaction potential between the cluster and daughter nucleus is expressed as

$$V_{\rm eff}(R) = \eta V_{\rm N}(R) + V_{\rm C}(R) + V_{\ell}(R)\,, \tag{1}$$

where η is the normalization factor, R represents the relative distance between the emitted cluster and daughter nucleus. The centrifugal term $V_{\ell}(R) = \frac{\hbar^2\ell(\ell+1)}{2\mu R^2}$, where ℓ denotes the orbital angular momentum quantum number and $\mu = A_{\rm c}A_{\rm d}/(A_{\rm c}+A_{\rm d})$ represents the reduced mass of the system. $A_{\rm c}$ and $A_{\rm d}$ are the mass numbers of the cluster and daughter nuclei, respectively. By considering the Langer modification, the following replacement can be made: $\ell(\ell+1) \to (\ell+\frac{1}{2})^2$. Langer-modified centrifugal barriers are employed in one-dimensional problems because they provide a more accurate and efficient method for solving quantum mechanical problems involving tunnelling through a potential barrier. This modification is particularly useful in one-dimensional problems as it regularizes the wave function and ensures that the WKB quantization condition is exact for the employed potentials [49, 50]. The quantum numbers ℓ were estimated based on combinations of the ground-state spin of the parent and daughter nuclei, employing the standard spin-parity selection rules [51]

$$|J_{\rm d} - J_{\rm p}| \;\le\; \ell \le J_{\rm d} + J_{\rm p}\,, \tag{2}$$

$$\pi_{\rm p} \;=\; (-1)^{\ell}\pi_{\rm d}\,. \tag{3}$$

The Coulomb potential $V_{\rm C}(R)$ is assumed to be the interaction between a point cluster and a uniformly charged spherical core

$$V_{\rm C}(R) = Z_{\rm c}Z_{\rm d}\frac{e^2}{4\pi\epsilon_0}\begin{cases} \frac{1}{R} & \text{for } R > R_{\rm C} \\ \frac{1}{2R_{\rm C}}\left[3 - \left(\frac{R}{R_{\rm C}}\right)^2\right] & \text{for } R \le R_{\rm C} \end{cases}. \tag{4}$$

Here, $Z_{\rm c}$ and $Z_{\rm d}$ represent the charge numbers of the cluster and daughter nuclei, respectively, and $R_{\rm C}$, which denotes the Coulomb radius, is determined from $R_{\rm C} = 1.2(A_{\rm c}^{1/3} + A_{\rm d}^{1/3})$.

In the DDCM framework, the nuclear interaction, $V_{\rm N}(R)$, between the cluster and daughter nuclei is obtained using

$$V_{\rm N}(R) = \int\int \rho_{\rm c}(\boldsymbol{r}_1)\xi(\rho)\rho_{\rm d}(\boldsymbol{r}_2)v_{NN}(E,s){\rm d}\boldsymbol{r}_1{\rm d}\boldsymbol{r}_2\,, \tag{5}$$

where $s = |R + \boldsymbol{r}_2 - \boldsymbol{r}_1|$ signifies the relative distance between the interacting nucleon pair, E represents the kinetic energy of the cluster particle, and $\rho_{\rm c}(\boldsymbol{r}_1)$ and $\rho_{\rm d}(\boldsymbol{r}_2)$ denote, respectively, the ground-state matter density distributions of the cluster and daughter nuclei. The matter density distributions used in this work have been estimated from wave functions of the relativistic mean-field theory, with the DD-ME2 parametrization [52].

In the relativistic mean-field theory, an atomic nucleus is considered to be a system composed of Dirac nucleons, exchange various mesons (σ, ω, and ρ) and the photon field (A_μ) through an effective Lagrangian given by [53–55]

$$\begin{aligned}\mathcal{L} = {} & \bar{\psi}_i \left\{ i\gamma^\mu \partial_\mu - M \right\} \psi_i + \frac{1}{2}\partial^\mu \sigma \partial_\mu \sigma - \frac{1}{2} m_\sigma^2 \sigma^2 - \frac{1}{3} g_2 \sigma^3 - \frac{1}{4} g_3 \sigma^4 \\ & - g_\sigma \bar{\psi}_i \psi_i \sigma - \frac{1}{4} \Omega^{\mu\nu} \Omega_{\mu\nu} + \frac{1}{2} m_\omega^2 \omega^\mu \omega_\mu - g_\omega \bar{\psi}_i \gamma^\mu \psi_i \omega_\mu - \frac{1}{4} \vec{B}^{\mu\nu} \cdot \vec{B}_{\mu\nu} \\ & + \frac{1}{2} m_\rho^2 \vec{\rho}^\mu \cdot \vec{\rho}_\mu - g_\rho \bar{\psi}_i \gamma^\mu \vec{\tau} \psi_i \cdot \vec{\rho}^\mu - \frac{1}{4} F^{\mu\nu} F_{\mu\nu} - e \bar{\psi}_i \gamma^\mu \left(\frac{1 - \tau_{3i}}{2} \right) \psi_i A_\mu \,, \end{aligned} \tag{6}$$

where parameters g_2, g_3, and $\frac{e^2}{4\pi}$ denote the nonlinear coupling constants. Moreover, the parameters g_σ, g_ω, and g_ρ are the respective coupling constants of the mesons whose corresponding masses are m_σ, m_ω and m_ρ, and M denotes the nucleon mass.

Using the variational principle, and after simplifications, the Dirac equation for nucleons is given by

$$[-i\alpha \nabla + \beta(M^* + g_\sigma \sigma) + g_\omega \omega + g_\rho \tau_3 \rho_3] \psi_i = \epsilon_i \psi_i \,. \tag{7}$$

Moroever, the Klein–Gordon equations governing the meson fields are obtained as

$$\begin{aligned} \left(-\nabla^2 + m_\sigma^2\right) \sigma(r) &= -g_\sigma \rho_s(r) - g_2 \sigma^2(r) - g_3 \sigma^3(r) \,, \\ \left(-\nabla^2 + m_\omega^2\right) V(r) &= g_\omega \rho(r) \,, \\ \left(-\nabla^2 + m_\rho^2\right) \rho(r) &= g_\rho \rho_3(r) \,. \end{aligned} \tag{8}$$

A self-consistent solution is obtained for Eqs. (7)–(8) that involves expanding the upper and lower components of the Dirac spinors and the boson fields within an axially deformed harmonic oscillator basis, with an initial deformation with the DD-ME2 force parameter. The baryon (vector) densities are determined using [52, 56]

$$\rho_v(r) = \sum_{i=1}^{\rm occ} \psi_i^\dagger(r) \psi_i(r) \,, \tag{9}$$

where the sums are taken over all the occupied (occ) states (for proton or neutron).

The M3Y-Reid and M3Y-Paris parametrizations, along with various NN interactions derived from relativistic mean-field theory (R3Y), have traditionally served as dependable choices for the analysis of cluster decay phenomena. Recent advancements have extended the utility of NN interactions obtained from relativistic mean theory (R3Y) to include alpha decay investigations [8, 11–13]. However, this study adopts the B3Y-Fetal NN interaction for the $v_{NN}(E,s)$ term, aiming to evaluate its efficacy in predicting the cluster decay half-lives of heavy and superheavy nuclei. The B3Y-Fetal NN interaction stems from the lowest-order constrained variational method [18] has been previously applied in symmetric nuclear matter computations [19], elastic scattering analyses [57], and alpha decay studies [58, 59]. In addition to its microscopic foundation, a notable distinction from the M3Y NN interactions lies in the Yukawa strengths of their central components. As elucidated in prior works [19, 57, 58], the B3Y-Fetal NN interaction can be expressed as

$$v_{NN}^{\mathrm{B3Y}}(E,s) = 10472.13\frac{e^{-4s}}{4s} - 2203.11\frac{e^{-2.5s}}{2.5s} + J_{00}(E)\delta(\boldsymbol{s})\,, \tag{10}$$

where

$$J_{00}(E) = -590(1 - 0.002E/A_{\mathrm{c}})\ \mathrm{MeV\ fm}^3 \tag{11}$$

denotes the zero-range exchange term, the energy released in the decay process is $E = Q_{\mathrm{c}}A_{\mathrm{c}}/A$, where A denotes the parent nucleus mass number.

The density-dependent term $\xi(\rho)$ of the NN interaction is given by

$$\xi(\rho) = C\left[1 + \alpha\exp\left(-\zeta\rho\right) - \gamma\rho^n\right]\,. \tag{12}$$

Here, five different density-dependent parametrizations have been employed. They include DDB3Y1, BDB3Y0, BDB3Y1, BDB3Y2, and BDB3Y3, and the parameters C, α, ζ, γ are those given in Refs. [19, 57] for the five parameter sets.

It should be noted that the present formalism does not explicitly incorporate microscopic shell corrections. Consequently, shell effects — such as the enhanced stability of magic or near-magic daughter nuclei — are not directly included in the calculated decay barrier or in the cluster preformation probability. This macroscopic nature of the model may lead to deviations in predicted lifetimes for decays involving strong shell closures. A more detailed treatment including shell-corrected potentials or microscopic preformation factors could further improve the predictive accuracy and will be explored in future work.

The Bohr–Sommerfeld quantization and Wildermuth rule [51, 60, 61]

$$\int_{R_1}^{R_2}\sqrt{\frac{2\mu}{\hbar}\left[Q_{\mathrm{c}} - V_{\mathrm{eff}}(R)\right]}\,\mathrm{d}R = (G_{\mathrm{c}} - \ell + 1)\,\frac{\pi}{2} \tag{13}$$

have been employed to determine the normalization factor η given in Eq. (1). In Eq. (13), the global quantum number $G_c = G_\alpha A_c/4$, where $G_\alpha = 22$ for $N > 126$, 20 for $82 < N \leq 126$, and it is 18 for $N \leq 82$. Moreover, R_1 and R_2 denote the first two turning points.

The half-life of the cluster decay can be calculated using the following expression:

$$T_{1/2} = \frac{\ln 2}{\nu P_c P}, \tag{14}$$

where the assault frequency, ν, is calculated using

$$\nu = \frac{\hbar}{2\mu}\left[\int_{R_1}^{R_2} \frac{\mathrm{d}R}{\sqrt{\frac{2\mu}{\hbar^2}\left|Q_c - V_{\mathrm{eff}}(R)\right|}}\right]^{-1}, \tag{15}$$

and the tunnelling probability, P, is determined using

$$P = \frac{1}{1 + \exp\left[\frac{\sqrt{8\mu}}{\hbar}\int_{R_2}^{R_3}\sqrt{V_{\mathrm{eff}}(R) - Q_c}\,\mathrm{d}R\right]}, \tag{16}$$

where R_3 denotes the third turning point, which is determined by numerically solving $V_{\mathrm{eff}}(R) - Q_c = 0$, and the cluster preformation probability, P_c, is known to contain important nuclear structure information.

The preformation probability has been shown to be connected to the shape of the interaction potential [62, 63]. Various empirical formulas have been given to obtain the cluster preformation probability [39, 63–65], some of the formulas depend on the cluster size A_c, while some depend on the Q_c value [64]. According to Santhosh and Jose [64], the preformation probability can be obtained using

$$\log_{10} P_c^{\mathrm{emp}} = aA_c + b, \tag{17}$$

where the parameters a and b were obtained as -0.51325 and 2.80787, respectively. In this study, we will compare the use of this preformation factor (denoted $\log_{10} P_c^{\mathrm{emp}}$) with the statistical preformation factor.

The cluster emissions of decaying parent nuclei in the trans-lead region are known to yield nearly spherical daughter nuclei at (or around) the shell closure. The daughter nucleus of mass A_d can be considered as the core of the parent nucleus of volume V with noninteracting nucleons orbiting this core and a cluster of volume v is emitted. The volume v is composed of Z_c protons and N_c neutrons and thus an emitted cluster is formed. Let the average neutron and proton number inside the volume v be represented as $\bar{N} = \rho_{0N}V$ and $\bar{Z} = \rho_{0Z}V$. The probability of N_c and Z_c forming within

volume v is determined by the grand-canonical distribution, which takes the expression [66, 67]

$$P_{N_c} = \frac{1}{N_c!}\exp^{-\bar{N}}(\bar{N})^{N_c}, \tag{18}$$

$$P_{Z_c} = \frac{1}{Z_c!}\exp^{-\bar{Z}}(\bar{Z})^{Z_c}. \tag{19}$$

The probability of cluster preformation takes the form

$$P_c = \frac{1}{N_c!}\exp^{-\bar{N}}(\bar{N})^{N_c}\frac{1}{Z_c!}\exp^{-\bar{Z}}(\bar{Z})^{Z_c}. \tag{20}$$

It is assumed that the same average nuclear density $\rho_0 = \rho_{0N} + \rho_{0Z}$ is shared between the parent nucleus and the emitted cluster instead of their respective $\rho = A/V \approx A_c/v$. Let the density ratio $x = \rho_0/\rho$, which means $\rho_0 = x\rho$. The cluster preformation probability (P_c) can be expressed as

$$\begin{aligned}\ln P_c = &-\ln N_c! - N_c x + N_c \ln N_c + N_c \ln x - \ln Z_c! \\ &-Z_c x + Z_c \ln Z_c + Z_c \ln x\,.\end{aligned} \tag{21}$$

By considering the Stirling formula, $\ln(N!) \approx N(\ln N - 1)$, Eq. (21) can be simplified as

$$\ln P_c = (1 - x + \ln x)N_c + (1 - x + \ln x)Z_c\,, \tag{22}$$

$$\log_{10} P_c = \frac{(1 - x + \ln x)A_c}{\ln 10}\,, \tag{23}$$

where the dimensionless quantity x denotes the nuclear density where the cluster is formed. The effect of this quantity will be subsequently discussed in Section 3.

3. Results and discussions

This section seeks to evaluate the application of the recently proposed B3Y-Fetal NN interaction and its density-dependent forms as described in Eqs. (5)–(12) on cluster radioactivity. This step is crucial as it provides the opportunity to examine the sensitivity of the calculated half-lives to the different B3Y-Fetal versions. It is worth noting that Eq. (5) is the expression for the double folding method which involves the integration of the matter density distribution over the B3Y-Fetal NN potential (Eq. (10)) whose zero-range exchange term is given in Eq. (11). The expression for the density-dependent term is given in Eq. (12). The matter density distribution of the participating nuclei is essential for the employed density-dependent cluster model. In the present work, the nucleon density distributions used in constructing the cluster–daughter interaction potential were obtained from a fully self-consistent relativistic mean-field (RMF) calculation.

The RMF framework is highly successful in describing the bulk properties of nuclei. The neutron and proton density distributions are widely recognized as valuable sources of information for understanding nuclear structure. They are particularly useful for identifying unique characteristics of nuclei, such as bubble formations, halo/skin structures, and cluster configurations. We have employed the DD-ME2 density-dependent meson-exchange parametrization, which has been shown to provide an accurate description of binding energies, deformations, and surface properties of medium and heavy nuclei. The proton, neutron, and total ground-state densities of the cluster and daughter nuclei were computed using the DIRHB code developed by Nikšić *et al.* [52]. This code solves the relativistic Hartree–Bogoliubov equations, and the resulting RMF densities are then directly incorporated into the density-dependent nucleon–nucleon interaction potential described in the previous section. The proton and neutron densities are obtained using Eq. (9).

The total density can be deduced by adding the proton and neutron densities. As a representative case, Fig. 1 shows the variation in the density distribution profiles of ^{14}C and ^{30}Mg clusters and of ^{210}Pb, and ^{204}Hg daughter nuclei as a function of the radial separation (r), calculated using RMF theory with the DD-ME2 parameter set. The proton, neutron, and total densities are shown in the plots. As shown in the figure, the density distribution of the light clusters ^{14}C and ^{30}Mg exhibits a peak in the central region, whereas those of the heavy mass ^{204}Hg and ^{210}Pb daughter nuclei manifest a depression in the central region. This disparity is attributed to the interplay between Coulomb repulsion and the nuclear shell structure [69, 70]. From a closer look at the figure, it can be deduced that the extent of central density depression has a close correlation with the mass of nucleons. In both cases, the central region is accompanied by a rapid fall in the surface region. Expectedly, the daughter nuclei possess a large neutron excess. While proton density primarily influences the surface region, neutron density predominantly affects the central depression or interior of the total density distribution of the nucleus.

To describe the spatial extent of the distribution of the positive charge in the participating nuclei, the root-mean-square charge radii of the cluster and daughter nuclei are shown in Table 1. The results are found to be in good agreement with available experimental data [68].

The total density is folded with the B3Y-Fetal interaction to obtain the effective nuclear cluster–daughter interaction V_{eff} as expressed in Eq. (5). Figure 2 describes the variation in V_{eff} for the B3Y-Fetal NN interactions and its different density-dependent versions with and without the inclusion of the normalization factor η for $^{238}\text{Pu} \rightarrow ^{28}\text{Mg} + ^{207}\text{Tl}$. A careful inspection of Fig. 2 (a) shows that V_{eff} is highly sensitive to the choice of the employed density-dependent parametrization. The effective interaction po-

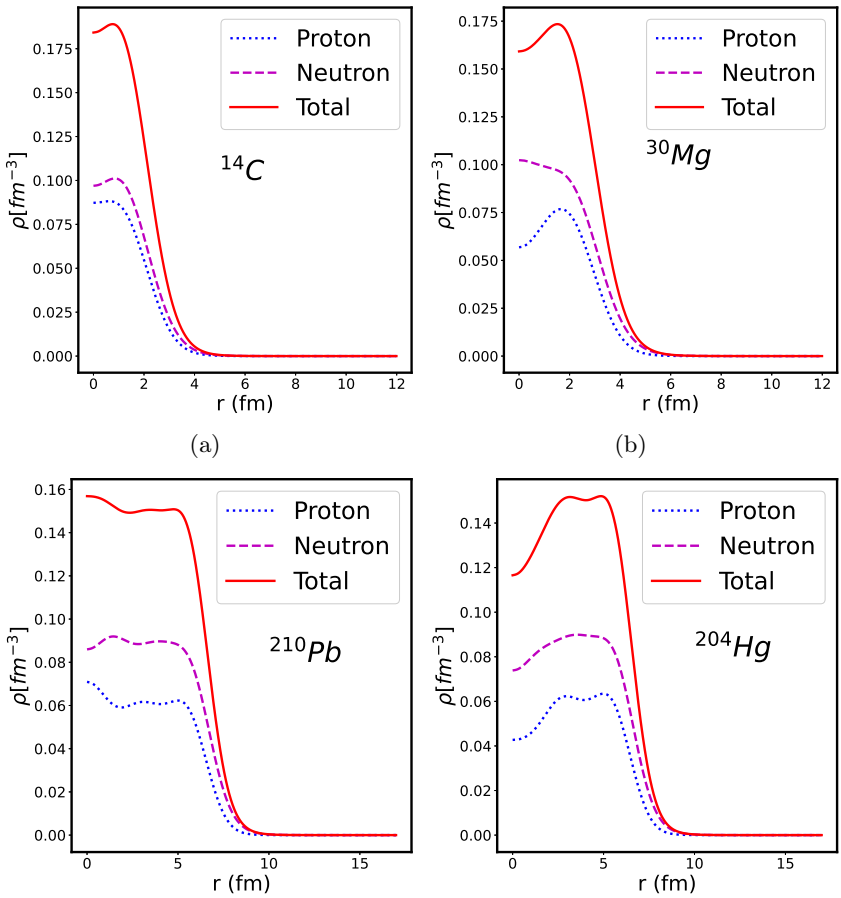

Fig. 1. Plots of the proton, neutron, and total densities for the cluster nuclei (a) ^{14}C, (b) ^{30}Mg, and daughter nuclei (c) ^{210}Pb and (d) ^{204}Hg, respectively.

tential is highly sensitive to the choice of the employed density-dependent parametrization because it directly affects the way the interaction between nucleons changes as the density of the system varies. The parametrization determines the functional forms (Eqs. (5) and (12)) and the strength of the interaction. We reiterate that B3Y-Fetal with no density-dependence is denoted DD0. On the other hand, the incorporation of density-dependent parametrizations DDB3Y1, BDB3Y0, BDB3Y1, BDB3Y2, and BDB3Y3 on the cluster–daughter potential, as indicated in Eq. (12) is known to reduce the potential strength. Here, the BDB3Y1 reproduced the deepest pocket. This infers that the BDB3Y1 relatively gives a more attractive core to NN potential among the considered parametrizations. However, Fig. 2 (b) clearly

reveals that the distinction in the strengths of the employed parametrization is eliminated with the inclusion of η. Beside the drastic reduction in the depth of the potential, it is apparent that there is no discernible difference in the predictions (with the inclusion of η), suggesting that these parameter sets will likely generate similar results.

Table 1. The root-mean-square charge radii for the cluster and daughter nuclei calculated using relativistic mean-field theory with DD-ME2 parametrization [52]. The results are compared to experimental data reported in Ref. [68].

Nucleus	Theory	Expt. [68]	Nucleus	Theory	Expt. [68]
^{14}C	2.5572	2.5025	^{211}Bi	5.5534	—
^{23}F	2.8252	—	^{204}Hg	5.4914	5.4744
^{28}Mg	3.0244	—	^{205}Hg	5.4952	5.4776
^{30}Mg	3.0691	—	^{206}Hg	5.4992	5.4837
^{22}Ne	2.8960	2.9525	^{207}Hg	5.5085	—
^{24}Ne	2.8842	2.9007	^{208}Hg	5.5178	—
^{25}Ne	2.9035	2.9316	^{207}Pb	5.5132	5.4943
^{26}Ne	2.9185	2.9251	^{208}Pb	5.5180	5.5012
^{18}O	2.7307	2.7726	^{209}Pb	5.5270	5.5100
^{20}O	2.7384	—	^{210}Pb	5.5360	5.5208
^{32}Si	3.1394	—	^{212}Pb	5.5538	5.5396
^{34}Si	3.1750	—	^{207}Tl	5.5088	5.4853

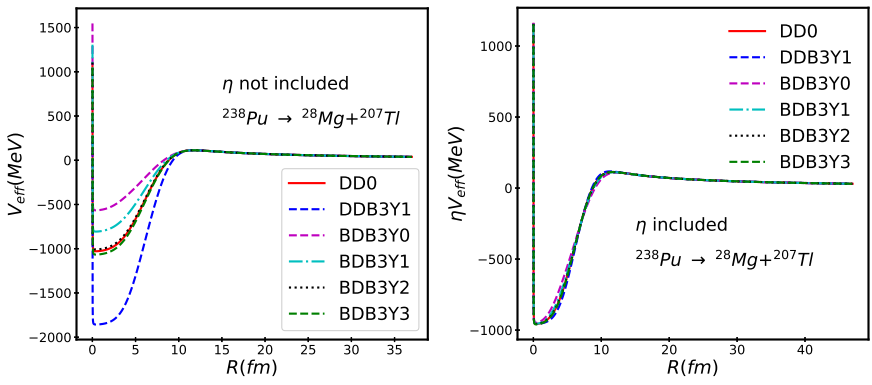

(a) (b)

Fig. 2. Variation of the B3Y-Fetal effective interaction potential V_{eff} using different parameter sets.

For validation purposes, Fig. 3 shows a comparison of the effective interaction potentials calculated using the B3Y-Fetal and the well-established M3Y-Reid NN interactions. DD0-B3Y and DD0-M3Y denote the potentials when no density-dependence is employed. As shown in Fig. 3 (a), the M3Y-Reid (DD0-M3Y) can be seen to give a more attractive core than the B3Y-Fetal (DD0-B3Y). However, when the density-dependent term is employed, the DDB3Y1 gives a stronger potential strength at the interior than the DDM3Y1. This shows the difference between the M3Y-Reid and B3Y-Fetal NN interactions. However, when the normalization is employed, no discernible difference is observed between the models, as shown in Fig. 3 (b).

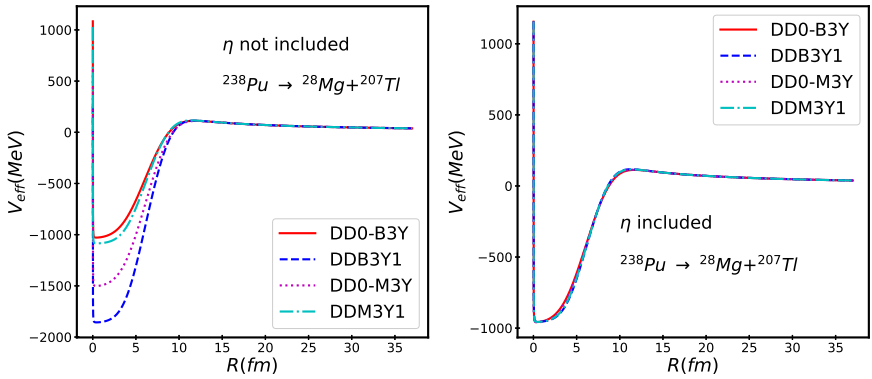

(a) (b)

Fig. 3. Comparison of the B3Y-Fetal and M3Y-Reid effective interaction potentials.

The relationship between the preformation probability and the cluster size in Eq. (17) is employed in the calculation of the decay half-lives of different cluster-emitting actinides within the range of $221 \leq A \leq 242$, as shown in Table 2. The angular momentum ℓ carried away by the emitted cluster, which is determined by combining the ground-state spin of the parent and daughter nuclei through the application of standard spin-parity selection rules, is shown in column three of the table. The decay energy (Q-values) in column four were extracted from the NUBASE2020 database [71], and values from Eq. (17) are given in column five in the logarithmic scale ($\log_{10} P_{\rm c}^{\rm emp}$). The experimentally measured half-lives and their corresponding theoretically calculated values using the B3Y-Fetal NN interaction termed (DD0) and its density-dependent versions (DDB3Y1, BDB3Y0, BDB3Y1, BDB3Y2, and BDB3Y3) are given in columns 6–12, respectively. From the table, it can be clearly observed that the experimental half-life data are well reproduced by the B3Y-Fetal interaction and its various density-dependent parameterizations. On the other hand, estimating the $P_{\rm c}$ from a statistical physics

framework could be highly useful for experimentally validated cluster decay and highly promising for easy extrapolation to the unknown region of the nuclear landscape.

Table 2. Cluster decay half-life calculations using B3Y-Fetal NN interaction with the cluster-mass-dependent preformation formula in Eq. (17).

Parent	Cluster	ℓ	Q_c	$\log P_c$	Expt.	DD0	DDB3Y1	BDB3Y0	BDB3Y1	BDB3Y2	BDB3Y3
^{221}Fr	^{14}C	3	31.291	−4.378	14.515	13.418	15.077	11.180	12.526	13.348	13.537
^{221}Ra	^{14}C	3	32.396	−4.378	13.319	12.238	13.880	10.002	11.350	12.168	12.356
^{222}Ra	^{14}C	0	33.049	−4.378	11.049	10.773	12.414	8.564	9.893	10.704	10.891
^{223}Ra	^{14}C	4	31.828	−4.378	15.045	13.265	14.895	11.041	12.390	13.195	13.382
^{224}Ra	^{14}C	0	30.534	−4.378	15.895	15.427	17.051	13.223	14.552	15.358	15.544
^{226}Ra	^{14}C	0	28.197	−4.378	21.288	20.328	21.936	18.140	19.460	20.260	20.444
^{225}Ac	^{14}C	4	30.476	−4.378	17.209	16.825	18.355	14.589	15.939	16.755	16.942
^{228}Th	^{20}O	0	44.723	−7.457	20.728	21.476	23.508	18.764	20.199	21.390	21.620
^{230}Th	^{24}Ne	0	57.760	−9.510	24.613	25.009	27.307	22.028	23.528	24.912	25.172
^{232}Th	^{26}Ne	0	55.912	−10.537	29.201	28.990	31.333	25.942	27.643	28.892	29.155
^{232}Th	^{24}Ne	0	54.668	−9.510	29.201	29.989	32.297	26.869	28.598	29.891	30.153
^{231}Pa	^{23}F	1	51.883	−8.997	26.017	24.434	26.612	21.479	23.263	24.342	24.588
^{231}Pa	^{24}Ne	1	60.410	−9.510	22.886	22.372	24.641	19.300	21.154	22.276	22.533
^{230}U	^{22}Ne	0	61.388	−8.484	19.561	20.373	22.571	17.463	18.874	20.279	20.530
^{232}U	^{24}Ne	0	62.309	−9.510	20.388	20.623	22.879	17.724	19.152	20.527	20.782
^{233}U	^{24}Ne	2	60.485	−9.510	24.844	23.427	25.676	20.332	22.205	23.330	23.586
^{234}U	^{24}Ne	0	58.825	−9.510	25.935	25.762	28.023	22.751	24.347	25.665	25.922
^{234}U	^{26}Ne	0	59.413	−10.537	25.935	25.851	28.152	22.762	24.499	25.753	26.013
^{234}U	^{28}Mg	0	74.111	−11.563	25.743	25.247	27.731	21.896	23.754	25.141	25.422
^{235}U	^{24}Ne	1	57.363	−9.510	27.444	28.205	30.460	25.062	26.971	28.108	28.365
^{235}U	^{25}Ne	3	57.683	−10.023	27.444	28.400	30.684	25.321	27.023	28.302	28.562
^{235}U	^{28}Mg	1	72.426	−11.563	27.444	27.716	30.189	24.331	26.377	27.610	27.891
^{237}Np	^{30}Mg	2	74.787	−12.590	27.228	27.043	29.509	23.696	25.719	26.938	27.217
^{236}Pu	^{28}Mg	0	79.670	−11.563	21.654	20.615	23.075	17.287	19.164	20.509	20.787
^{238}Pu	^{28}Mg	0	75.911	−11.563	25.664	25.023	27.873	22.041	23.977	24.942	25.595
^{238}Pu	^{30}Mg	0	76.793	−12.590	25.664	25.117	27.883	22.072	24.031	25.033	25.256
^{238}Pu	^{32}Si	0	91.187	−13.616	25.296	25.383	28.347	22.083	24.206	25.292	25.535
^{242}Cm	^{34}Si	0	96.544	−14.643	23.107	23.026	25.856	19.493	21.725	22.925	23.195

The statistical cluster preformation probability formula equation (23) proposed by Dong *et al.* [43] in terms of the nuclear density is employed in the present study. It is noteworthy that this expression keenly follows the Blendowske and Walliser scaling (spectroscopic) factor [65]. Table 3 shows the values of the density ratio x in Eq. (23) for the various density-dependent versions of the B3Y-Fetal NN interaction using the least square fitting method for the experimentally measured half-lives of 28 cluster emitters. It is interesting to note that all the obtained values align with those of Dong *et al.* [43] and Santhosh and Angali [72] who estimated $x = 0.20$ and $x = 0.18$, respectively. The authors reported that these values are within the vicinity of < 0.18 having a density less than 0.03 fm^3, predicted in Ref. [73]

in the nuclear matter calculation of α-clustering. This conjecture presupposes that cluster formation occurs at the nuclear surface where the nuclear matter has a lower density.

Table 3. Value of x from Eq. (23).

Model	DD0	DDB3Y1	BDB3Y0	BDB3Y1	BDB3Y2	BDB3Y3
Calculated x	0.170	0.223	0.123	0.148	0.169	0.174

To further validate the applicability of the statistical preformation probability in describing cluster radioactivity, the values from the cluster size-based preformation probability in P_c^{emp} are compared with those of P_c^{stat} in a logarithmic scale in Fig. 4. As shown in the figure, a close agreement is seen between DD0, BDB3Y2, BDB3Y3 and $\log_{10} P_c^{\text{emp}}$, and thus, their half-life predictions could be somewhat relative. It is also observed that for the preformation of ^{14}C cluster, there is a keen agreement between the DDB3Y1 and the $\log_{10} P_c^{\text{emp}}$ while a large deviation is seen in their predictions for other systems. The peculiarity of systems emitting ^{14}C cluster

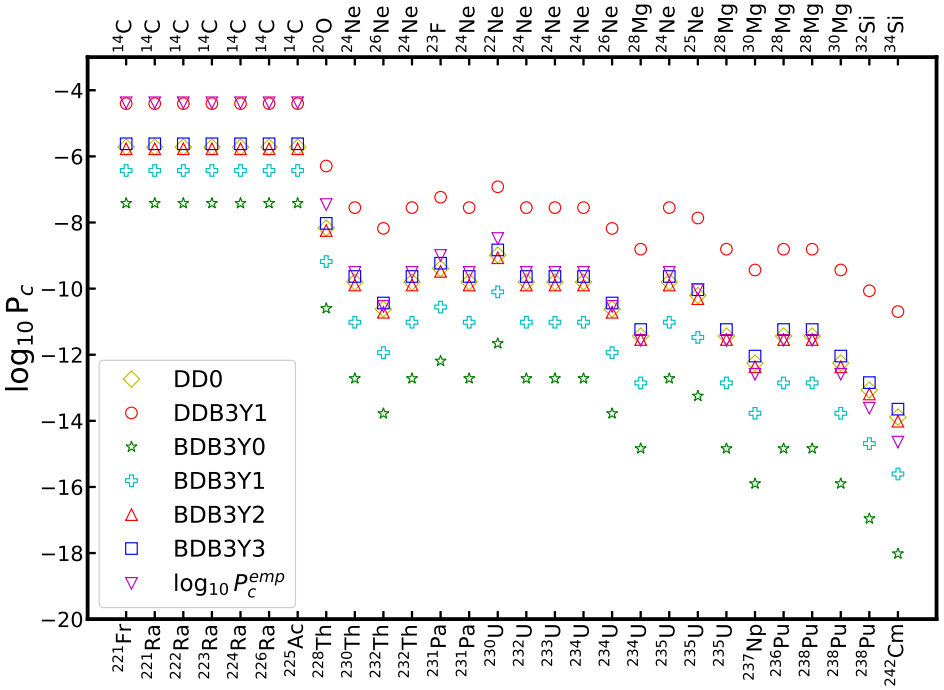

Fig. 4. The calculated preformation factors using Eq. (22) with the six density-dependent B3Y parametrizations compared with the empirical preformation factor given in Eq. (17).

(which is a strongly bound nucleus with $N/Z = 1.33$) and similar deviations has been previously reported based on the choice of the employed proximity potential and neck-length parameter [15, 74, 75]. Thus, this study complements the previous findings that the variability or choice of NN potential could also address and influence the accurate reproduction of the decay half-lives of such systems. Although the difference between the BDB3Y1 ($P_{\mathrm{c}}^{\mathrm{stat}}$) and $\log_{10} P_{\mathrm{c}}^{\mathrm{emp}}$ is significantly large, the results obtained from the BDB3Y1, BDB3Y0, BDB3Y2, BDB3Y3, DD0, and DDB3Y1, are in good agreement with the extracted preformation factor, which are not shown in the figure in order to avoid the ambiguity of presentation.

Table 4 shows the calculated cluster decay half-lives using the B3Y-Fetal NN interaction with statistical preformation factor in Eq. (23). The first column of the table outlines the decaying parent nuclei and the second column shows their respective emitted cluster. For these energetically favoured decays, the experimental decay half-lives are shown in column three. The calculated half-lives shown in columns 4–9 are found to be close to the experimentally measured data. To evaluate the predictive accuracy of the cluster size-based preformation probability in Eq. (17) and the statistical preformation factor in Eq. (23), the degree of agreement between the calculated decay half-lives and the experimental data is evaluated by using the root-mean-square error (RMSE)

$$\mathrm{RMSE} = \sqrt{\frac{1}{N}\sum_{i=1}^{N}\left[\left(\log_{10} T_{1/2,i}^{\mathrm{expt}} - \log_{10} T_{1/2,i}^{\mathrm{calc}}\right)^2\right]}, \tag{24}$$

where $\log_{10} T_{1/2,i}^{\mathrm{expt}}$ and $\log_{10} T_{1/2,i}^{\mathrm{calc}}$ are the logarithmic forms of the experimental and calculated half-lives (from $\log_{10} P_{\mathrm{c}}^{\mathrm{emp}}$ and $\log_{10} P_{\mathrm{c}}^{\mathrm{stat}}$), respectively. Table 5 displays the tabulated RMSE of the half-lives using the B3Y-Fetal NN interaction and its density-dependent parametrizations.

In most cases, it is evident that the calculated half-lives with the statistical preformation probability yield relatively lower RMSE values, indicating better agreement with the experimentally observed values. However, there is an exception with DD0 and BDB3Y3, where the RMSE for the cluster size-based preformation probability is found to be slightly lower than that of the statistical preformation probability with a difference of 0.024 and 0.0645, respectively. Thus, this result asserts the reliability of the statistical preformation probability and suggests that it can compete with the well-known cluster size-based preformation probability, and sometimes outperform it, in terms of predictive accuracy.

Table 4. Cluster decay half-life calculations using B3Y-Fetal NN interaction with statistical preformation factor in Eq. (22).

Parent nucleus	Emitted cluster	$\log_{10} T_{1/2}(s)$						
		Expt	DD0	DDB3Y1	BDB3Y0	BDB3Y1	BDB3Y2	BDB3Y3
^{221}Fr	^{14}C	14.515	14.758	15.103	14.222	14.575	14.740	14.779
^{221}Ra	^{14}C	13.319	13.578	13.906	13.044	13.399	13.561	13.598
^{222}Ra	^{14}C	11.049	12.113	12.440	11.606	11.942	12.096	12.132
^{223}Ra	^{14}C	15.045	14.604	14.921	14.083	14.439	14.587	14.623
^{224}Ra	^{14}C	15.895	16.767	17.077	16.265	16.601	16.750	16.785
^{226}Ra	^{14}C	21.288	21.668	21.962	21.182	21.509	21.652	21.685
^{225}Ac	^{14}C	17.209	18.165	18.381	17.632	17.988	18.147	18.184
^{228}Th	^{20}O	20.728	22.186	22.342	21.907	21.923	22.175	22.190
^{230}Th	^{24}Ne	24.613	25.300	25.346	25.237	25.035	25.293	25.295
^{232}Th	^{26}Ne	29.201	29.072	28.975	29.185	29.041	29.071	29.054
^{232}Th	^{24}Ne	29.201	30.280	30.336	30.079	30.105	30.272	30.276
^{231}Pa	^{23}F	26.017	24.830	24.850	24.672	24.824	24.824	24.823
^{231}Pa	^{24}Ne	22.886	22.663	22.680	22.510	22.661	22.657	22.655
^{230}U	^{22}Ne	19.561	20.874	21.008	20.639	20.490	20.862	20.876
^{232}U	^{24}Ne	20.388	20.914	20.918	20.934	20.659	20.908	20.905
^{233}U	^{24}Ne	24.844	23.718	23.715	23.542	23.712	23.711	23.709
^{234}U	^{24}Ne	25.935	26.053	26.062	25.960	25.854	26.046	26.045
^{234}U	^{26}Ne	25.935	25.932	25.794	26.004	25.898	25.932	25.911
^{234}U	^{28}Mg	25.743	25.119	24.975	25.172	25.044	25.118	25.097
^{235}U	^{24}Ne	27.444	28.496	28.500	28.272	28.478	28.489	28.488
^{235}U	^{25}Ne	27.444	28.586	28.525	28.547	28.476	28.582	28.572
^{235}U	^{28}Mg	27.444	27.587	27.433	27.607	27.667	27.586	27.566
^{237}Np	^{30}Mg	27.228	26.705	26.357	27.005	26.901	26.712	26.668
^{236}Pu	^{28}Mg	21.654	20.486	20.320	20.563	20.454	20.486	20.463
^{238}Pu	^{28}Mg	25.664	24.894	25.117	25.317	25.267	24.919	25.270
^{238}Pu	^{30}Mg	25.664	24.779	24.730	25.382	25.213	24.807	24.707
^{238}Pu	^{32}Si	25.296	24.835	24.797	25.426	25.279	24.864	24.762
^{242}Cm	^{34}Si	23.107	22.268	21.909	22.870	22.690	22.295	22.199

Table 5. The root-mean-square error of the half-lives calculated using the B3Y-Fetal NN interaction, with different parametrizations using the cluster-mass-dependent preformation formula in Eq. (17) and the statistical preformation factor in Eq. (22).

Model	DD0	DDB3Y1	BDB3Y0	BDB3Y1	BDB3Y2	BDB3Y3
$\log_{10} P_{\rm c}^{\rm emp}$ [Eq. (17)]	0.7898	2.1410	3.2513	1.6250	0.8217	0.7520
$\log_{10} P_{\rm c}$ [Eq. (22)]	0.8138	0.9202	0.6855	0.6875	0.8059	0.8165

For intuitive comparison, the deviation between the logarithm of the calculated cluster decay half-lives and the experimental half-lives for the six density-dependent B3Y parametrizations — DD0 (dark yellow diamond), DDB3Y1 (red circle), BDB3Y0 (green star), BDB3Y1 (blue plus sign), BDB3Y2 (red triangle), and BDB3Y3 (blue rectangle) is graphically illustrated in Fig. 5. It is evident that the variances between the majority of the calculated data points and the experimental data fall within the range of 1 to −1 of the general trend. Moreover, all the calculated data points fall within the range ±2.

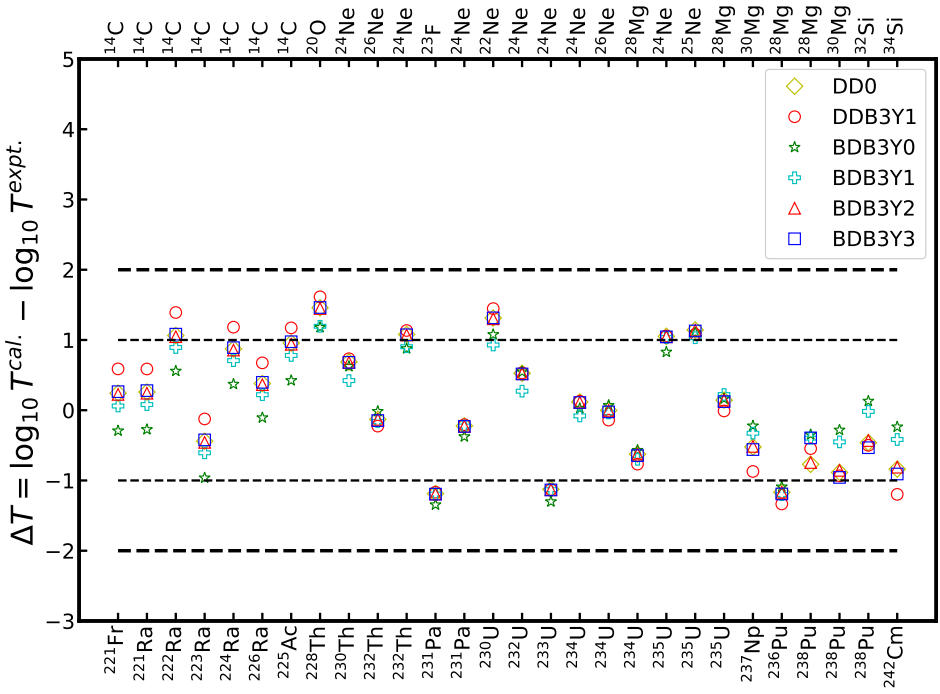

Fig. 5. The deviation between the logarithm of the calculated cluster decay half-lives and the experimental half-lives $\left(\Delta T = \log_{10}\left[T_{1/2}^{\mathrm{cal}}\right] - \log_{10}\left[T_{1/2}^{\mathrm{expt}}\right]\right)$, for the six density-dependent B3Y parameterizations, using the statistical preformation probability.

The successful agreement between the calculated half-lives using various B3Y-Fetal parametrizations and experimentally measured cluster decay half-lives spurs us to extend this theoretical investigation to predict the half-lives of energetically favoured but unobserved cluster radioactive decays, as illustrated in Table 6. In principle, the preformation, penetration probabilities, and decay constants will undergo significant modifications, leading to

Table 6. Predicted cluster decay half-lives using the BDB3Y1 and BDB3Y2 parameter sets, and the statistical preformation factor. Comparison with previous theoretical predictions of Refs. [17] and [76] is presented.

							$\log_{10}[T_{1/2}(s)]$			
A	Z	A_c	Z_c	Q_c	$\log_{10} P_c^{BDB3Y0}$	$\log_{10} P_c^{BDB3Y1}$	BDB3Y0	BDB3Y1	NL2 [17]	MGLDM [76]
220	88	12	6	32.0202	−6.3598	−5.5086	11.1525	11.6278	11.57991	12.14
226	88	20	8	40.8166	−10.5997	−9.1809	26.8133	27.0767	26.35602	25.72
224	90	15	7	38.1519	−7.9497	−6.8857	17.0983	17.3227	18.27131	17.91
224	90	24	10	55.4497	−12.7196	−11.0171	29.3261	29.2207	29.52504	27.84
226	90	15	7	34.9555	−7.9497	−6.8857	22.8833	23.4444	22.60753	23.11
226	90	24	10	56.4946	−12.7196	−11.0171	27.5291	27.3606	26.97113	26.52
228	90	24	10	57.4127	−12.7196	−11.0171	25.9514	25.7491	25.48976	25.72
229	90	21	8	43.2725	−11.1296	−9.6400	25.4257	25.5447	25.21418	23.22
232	91	25	10	59.0159	−13.2496	−11.4762	25.1675	24.9253	24.24358	23.38
232	91	28	12	71.2944	−14.8395	−12.8533	27.7443	27.6223	28.14344	27.29
230	92	20	8	43.7718	−10.5997	−9.1809	25.9697	26.2048	25.36608	25.37
230	92	24	10	61.3521	−12.7196	−11.0171	22.4851	22.2364	21.9369	23.28
230	92	32	14	85.5966	−16.9595	−14.6895	29.7739	29.5534	30.96135	29.9
232	92	28	12	74.3197	−14.8395	−12.8533	25.0950	24.9412	25.66872	25.1
234	92	27	11	64.6973	−14.3095	−12.3943	28.7673	28.6987	29.13987	28.46
234	93	28	12	77.2277	−14.8395	−12.8533	22.5441	22.4044	22.86723	23.59
236	93	29	12	75.0261	−15.3695	−13.3124	25.9449	25.7989	25.12014	26.1
234	94	27	11	65.9224	−14.3095	−12.3943	29.8776	29.8626	30.23928	30.01
234	94	29	13	82.3787	−15.3695	−13.3124	26.7722	26.7050	27.94482	27.45
236	94	24	10	59.2226	−12.7196	−11.0171	28.0801	28.0627	26.71367	28.31
236	94	29	13	82.1438	−15.3695	−13.3124	26.8932	26.8474	28.03247	27.82
238	95	29	12	77.2913	−15.3695	−13.3124	25.6784	25.5821	24.73797	26.06
238	95	33	14	92.7555	−17.4894	−15.1486	25.8158	25.6384	26.23359	27.76
240	95	34	14	93.7560	−18.0194	−15.6076	24.9880	24.7693	25.31086	25.42
238	96	32	14	97.3076	−16.9595	−14.6895	21.3290	21.2336	21.84239	23.34
240	96	30	12	76.5587	−15.8995	−13.7714	28.8031	28.7038	28.24278	26.4
240	96	34	14	95.5013	−18.0194	−15.6076	24.3823	24.1995	25.23913	25.21
242	96	32	14	93.6099	−16.9595	−14.6895	25.2917	25.2214	24.57478	25.96
220	88	16	8	39.6989	−8.4797	−7.3448	24.7332	25.3219	26.90552	24.98
222	88	15	7	35.2532	−7.9497	−6.8857	20.4035	20.7995	21.86033	20.44
224	88	20	8	39.7198	−10.5997	−9.1809	29.1305	29.5139	28.95545	28.56
224	90	14	6	32.9279	−7.4198	−6.4267	13.6088	13.9685	14.15419	13.64
224	90	16	8	46.4803	−8.4797	−7.3448	15.3862	15.4210	16.8809	19.38
226	90	14	6	30.5473	−7.4198	−6.4267	18.1518	18.5077	18.66503	17.72
226	90	18	8	45.7291	−9.5397	−8.2628	18.4195	18.4290	17.74797	17.85
228	90	14	6	28.2208	−7.4198	−6.4267	23.1807	23.5277	24.09264	22.31
232	91	27	11	63.7514	−14.3095	−12.3943	28.8779	28.7787	29.14489	28.35
230	92	14	6	28.3417	−7.4198	−6.4267	24.9583	25.3237	26.11331	24.04
230	92	21	9	49.9211	−11.1296	−9.6400	27.4032	27.5836	26.38161	26.99
230	92	28	12	73.9801	−14.8395	−12.8533	25.6998	25.5241	26.03443	26.85
232	92	23	9	49.5818	−12.1896	−10.5581	29.8797	30.0310	29.49255	28.65
232	92	32	14	85.2867	−16.9595	−14.6895	30.0551	29.8579	29.85732	29.63

continued

234	93	25	10	60.2485	−13.2496	−11.4762	25.8358	25.6600	24.87428	23.99
236	93	28	12	75.1494	−14.8395	−12.8533	25.1416	25.0458	24.32678	25.77
236	93	30	12	74.5141	−15.8995	−13.7714	27.3450	27.1536	26.53448	26.84
234	94	24	10	62.2547	−12.7196	−11.0171	23.6337	23.4424	22.95931	24.45
234	94	28	12	79.1555	−14.8395	−12.8533	21.4301	21.3143	22.17302	22.6
234	94	32	14	91.7729	−16.9595	−14.6895	25.1231	24.9224	25.03391	26.25
236	94	27	11	66.6780	−14.3095	−12.3943	28.5404	28.5132	28.79867	28.94
236	94	32	14	91.6695	−16.9595	−14.6895	25.0844	24.9130	25.30274	25.98
238	94	31	13	82.1484	−16.4295	−14.2305	27.9747	27.8366	28.03651	28.19
238	95	28	12	78.2321	−14.8395	−12.8533	23.8060	23.7477	22.79609	24.94
238	95	32	14	94.7513	−16.9595	−14.6895	22.8208	22.6871	22.8516	23.76
240	95	33	14	93.0598	−17.4894	−15.1486	25.2330	25.0680	25.60342	27.27
238	96	28	12	80.4173	−14.8395	−12.8533	22.5006	22.4407	22.95752	23.99
240	96	32	14	97.5504	−16.9595	−14.6895	20.8440	20.7547	21.32249	22.67
242	96	34	14	96.5439	−18.0194	−15.6076	22.9220	22.7425	23.70909	23.98
242	98	32	14	99.4175	−16.9595	−14.6895	21.8060	21.7493	21.99742	24.32

notable changes in the cluster-decay half-lives. In Table 6, columns 1 and 2 contain the mass number and charge number of the decaying parent nuclei, respectively, while columns 3 and 4 provide the information on the emitted clusters. The Q-values (Q_c) are given in column 5 and the statistical preformation probability in Eq. (23) is employed for the estimation of the values in columns 6 and 7 (in a logarithmic scale). The predictions using the BDB3Y0 and BDB3Y1 parametrizations presented in columns 8 and 9 are found to be consistent with earlier predictions from the relativistic R3Y-NL2 interactions [17] in column 10 and the modified generalized liquid drop model (MGLDM) [76] in column 11. Interestingly, the predicted half-life values fall below 10^{30} seconds, which is the experimental upper limit. Thus, these predictions can serve as a guide for future experimental endeavours. This not only validates the application of the B3Y-Fetal interaction to cluster radioactivity but also gives credence to the use of the statistical preformation factor.

It should be noted that many of the daughter nuclei in this study are known to exhibit significant quadrupole deformation. Since the present calculation assumes spherical symmetry, the possible influence of deformation on the preformation probability $\log_{10} P$ and the decay half-life $\log_{10} T_{1/2}$ is not explicitly included. Nuclear deformation modifies both the nuclear density distribution and the shape of the interaction potential, which in turn can alter the barrier height, barrier width, and the overlap between the cluster and the parent nucleus. Consequently, the omission of deformation may lead to quantitative differences in the predicted values of $\log_{10} P$ and $\log_{10} T_{1/2}$, especially for strongly deformed systems. Including deformation-dependent potentials or deformation-corrected preformation factors would likely improve the accuracy of the model and represents an important avenue for future work.

4. Conclusion

We have studied the application of B3Y-Fetal NN interactions and their various density-dependent parametrizations on cluster radioactivity. The cluster preformation probability is obtained from the statistical physics framework, which incorporates the density ratio that reveals the site of the cluster formation (at the nuclear surface). In comparison with the empirical cluster mass-dependent formula, the BDB3Y1, BDB3Y0, BDB3Y2, BDB3Y3, DD0, and DDB3Y1 were found to aptly reproduce the experimentally measured half-lives. Particularly, the root-mean-square error in the calculated half-lives of the BDB3Y1 and BDB3Y0 with the $P_{\mathrm{c}}^{\mathrm{stat}}$ were estimated to be 0.6875 and 0.6855, respectively, indicating a better predictive power over the well-known $P_{\mathrm{c}}^{\mathrm{emp}}$ with values 1.6250 and 3.2513. These findings allude to the applicability of the B3Y-Fetal interaction, and the statistical probability seems promising to study cluster radioactive decays in the unknown region of the nuclear territory. Interestingly, this work complements the previous findings in the literature about the peculiarity of ^{14}C cluster decay. Besides the known influence of the proximity potential and modification of the entrance channel through the neck-length, we have demonstrated here that the choice of NN potential can also influence the accurate fitting of the cluster preformation and hence the half-lives. From our calculations, the DDB3Y1 density-dependent parametrization was found to keenly address the deviations known with ^{14}C decays. Extending this theoretical investigation to predict the half-lives of energetically favoured but unobserved cluster radioactive decays results in half-life values falling below 10^{30}s, which is the experimental upper limit. Consequently, these predictions can serve as a guide for future experimental endeavours.

REFERENCES

[1] M. Hjorth-Jensen, T.S. Kuo, E. Osnes, «Realistic effective interactions for nuclear systems», *Phys. Rep.* **261**, 125 (1995).

[2] M. Freer, «Clustering in Light Nuclei; from the Stable to the Exotic», in: C. Scheidenberger, M. Pfützner (Eds.) «The Euroschool on Exotic Beams, Vol. IV. Lecture Notes in Physics, Vol. 879», *Springer*, Berlin, Heidelberg 2014.

[3] G. Bertsch, J. Borysowicz, H. McManus, W.G. Love, «Interactions for inelastic scattering derived from realistic potentials», *Nucl. Phys. A* **284**, 399 (1977).

[4] N. Anantaraman, H. Toki, G.F. Bertsch, «An effective interaction for inelastic scattering derived from the Paris potential», *Nucl. Phys. A* **398**, 269 (1983).

[5] D.T. Khoa, G.R. Satchler, W. Von Oertzen, «Nuclear incompressibility and density dependent NN interactions in the folding model for nucleus–nucleus potentials», *Phys. Rev. C* **56**, 954 (1997).

[6] C. Lahiri, S.K. Biswal, S.K. Patra, «Effects of NN potentials on p nuclides in the $A \approx 100$–120 region», *Int. J. Mod. Phys. E* **25**, 1650015 (2016).

[7] B. Singh, M. Bhuyan, S.K. Patra, R.K. Gupta, «Optical potential obtained from relativistic-mean-field theory-based microscopic nucleon–nucleon interaction: applied to cluster radioactive decays», *J. Phys. G: Nucl. Part. Phys.* **39**, 025101 (2012).

[8] J.T. Majekodunmi *et al.*, «Decay Properties of ^{253,255}Rf using the Relativistic Mean-Field Framework Within the Preformed Cluster-Decay Model», *Phys. Part. Nuclei Lett.* **20**, 1361 (2023).

[9] S. Rana, M. Bhuyan, R. Kumar, «Systematic study of fusion barrier characteristics within the relativistic mean-field formalism», *Phys. Rev. C* **105**, 054613 (2022).

[10] S. Rana *et al.*, «Investigation of Astrophysical S-Factor for $^{12}\mathrm{C} + {}^{16}\mathrm{O}$ and $^{16}\mathrm{O} + {}^{16}\mathrm{O}$ Reactions Within the Relativistic Mean-Field Approach», *ECS Trans.* **107**, 12451 (2022).

[11] M. Das *et al.*, «Structure and decay chain of fermium isotopes using relativistic mean-field approach», *Mod. Phys. Lett. A* **37**, 2250133 (2022).

[12] W.A. Yahya, I.D. Olusola, A.A. Saeed, O.K. Azeez, «Half-lives of α-decay from nuclei with $Z = 92$–118 using the double folding model with relativistic NN interactions», *Nucl. Phys. A* **1018**, 122360 (2022).

[13] W.A. Yahya, K.J. Oyewumi, «Calculations of the Alpha Decay Half-lives of Some Polonium Isotopes Using the Double Folding Model», *Acta Phys. Pol. B* **52**, 1357 (2021).

[14] J.T. Majekodunmi *et al.*, «Cluster decay half-lives of $^{112-122}$Ba isotopes from the ground state and intrinsic excited state using the relativistic mean-field formalism within the preformed-cluster-decay model», *Phys. Rev. C* **105**, 044617 (2022).

[15] J.T. Majekodunmi *et al.*, «Preformation probability and kinematics of clusters emission yielding Pb-daughters», *Chinese Phys. C* **47**, 074106 (2023).

[16] J.T. Majekodunmi, R. Kumar, M. Bhuyan, «Quest for a universal cluster preformation formula: A new paradigm for estimating the cluster formation energy», *Europhys. Lett.* **143**, 24001 (2023).

[17] W.A. Yahya, T.T. Ibrahim, «Cluster decay half-lives using relativistic density dependent double folding model», *Eur. Phys. J. A* **58**, 48 (2022).

[18] J.O. Fiase, K.R.S. Devan, A. Hosaka, «Mass dependence of M3Y-type interactions and the effects of tensor correlations», *Phys. Rev. C* **66**, 014004 (2002).

[19] I. Ochala, J.O. Fiase, «Symmetric nuclear matter calculations: A variational approach», *Phys. Rev. C* **98**, 064001 (2018).

[20] D.N. Basu, «Nuclear incompressibility using the density-dependent M3Y effective interaction», *J. Phys. G: Nucl. Part. Phys.* **30**, B7 (2004).

[21] L.W. Chen *et al.*, «Incompressibility of Asymmetric Nuclear Matter», *Int. J. Mod. Phys. E* **19**, 1675 (2010).

[22] J.T. Majekodunmi *et al.*, «Systematic Analysis for Neck-Length and Q-Values on Cluster Decay from Ba Isotopes», *ECS Trans.* **107**, 2893 (2022).

[23] L.J. Qi *et al.*, «Systematic calculations of cluster radioactivity half-lives in trans-lead nuclei», *Chinese Phys. C* **47**, 014101 (2023).

[24] A. Sandulescu, D.N. Poenaru, W. Greiner, *Sov. J. Part. Nucl.* **11**, 528 (1980).

[25] H.J. Rose, G.A. Jones, «A new kind of natural radioactivity», *Nature* **307**, 245 (1984).

[26] R. Bonetti, A. Guglielmetti, «Cluster radioactivity: An overview after twenty years», *Rom. Rep. Phys.* **59**, 301 (2007).

[27] K. Wei, H.F. Zhang, «α decay and cluster radioactivity within the redefined preformed cluster method», *Phys. Rev. C* **102**, 034318 (2020).

[28] D.N. Poenaru, R.A. Gherghescu, W. Greiner, «Single universal curve for cluster radioactivities and α decay», *Phys. Rev. C* **83**, 014601 (2011).

[29] O.A.P. Tavares, E.L. Medeiros, «Natural and artificial alpha radioactivity of platinum isotopes», *Phys. Scr.* **84**, 045202 (2011).

[30] Y.L. Zhang, Y.Z. Wang, «Systematic study of cluster radioactivity of superheavy nuclei», *Phys. Rev. C* **97**, 014318 (2018).

[31] D.N. Poenaru, M. Ivascu, A. Sandulescu, W. Greiner, «Spontaneous emission of heavy clusters», *J. Phys. G: Nucl. Phys.* **10**, L183 (1984).

[32] W. Greiner, M. Ivascu, D.N. Poenaru, A. Sandulescu, «On exotic nuclear decay of ^{223}Ra by emission of ^{14}C nuclei», *Z. Physik A* **320**, 347 (1985).

[33] G. Royer, R.K. Gupta, V.Y. Denisov, «Cluster radioactivity and very asymmetric fission through compact and creviced shapes», *Nucl. Phys. A* **632**, 275 (1998).

[34] S. Kumar *et al.*, «The formation and decay of superheavy nuclei produced in ^{48}Ca-induced reactions», *J. Phys. G: Nucl. Part. Phys.* **29**, 625 (2003).

[35] S. Kumar, R. Rani, R. Kumar, «Shell closure effects studied via cluster decay in heavy nuclei», *J. Phys. G: Nucl. Part. Phys.* **36**, 015110 (2009).

[36] M. Balasubramaniam, R.K Gupta, «Heavy-ion emission in spontaneous decays of ^{249,252}Cf nuclei», *Phys. Rev. C* **60**, 064316 (1999).

[37] M. Balasubramaniam, S. Kumarasamy, N. Arunachalam, R.K. Gupta, «New semiempirical formula for exotic cluster decay», *Phys. Rev. C* **70**, 017301 (2004).

[38] M. Horoi, «Scaling behaviour in cluster decay», *J. Phys. G: Nucl. Part. Phys.* **30**, 945 (2004).

[39] Z. Ren, C. Xu, Z. Wang, «New perspective on complex cluster radioactivity of heavy nuclei», *Phys. Rev. C* **70**, 034304 (2004).

[40] D. Ni, Z. Ren, T. Dong, C. Xu, «Unified formula of half-lives for α decay and cluster radioactivity», *Phys. Rev. C* **78**, 044310 (2008).

[41] M. Balasubramaniam, N.S. Rajeswari, «An empirical relation for cluster decay preformation probability», *Int. J. Mod. Phys. E* **23**, 1450018 (2014).

[42] Y. Qian, Z. Ren, «Unified description of α-decay and cluster radioactivity in the trans-tin region», *J. Phys. G: Nucl. Part. Phys.* **39**, 015103 (2012).

[43] J.M. Dong, H.F. Zhang, J.Q. Li, W. Scheid, «Cluster preformation in heavy nuclei and radioactivity half-lives», *Eur. Phys. J. A* **41**, 197 (2009).

[44] G.R. Satchler, W.G. Love, «Folding model potentials from realistic interactions for heavy-ion scattering», *Phys. Rep.* **55**, 183 (1979).

[45] Z. Ren, C. Xu, Z. Wang, «New perspective on complex cluster radioactivity of heavy nuclei», *Phys. Rev. C* **70**, 034304 (2004).

[46] C. Xu, Z. Ren, «Systematical calculation of α decay half-lives by density-dependent cluster model», *Nucl. Phys. A* **753**, 174 (2005).

[47] Y. Qian, Z. Ren, D. Ni, «Reexamining cluster radioactivity in trans-lead nuclei with consideration of specific density distributions in daughter nuclei and clusters», *Phys. Rev. C* **94**, 024315 (2016).

[48] Z. Wang, Z. Ren, «Effects of nuclear surface polarization on exotic cluster radioactivity in trans-lead nuclei», *Phys. Rev. C* **108**, 024306 (2023).

[49] B.-F. Li, T. Zhu, A. Wang, «Langer Modification, Quantization Condition and Barrier Penetration in Quantum Mechanics», *Universe* **6**, 90 (2020).

[50] J.J. Morehead, «Asymptotics of radial wave equations», *J. Math. Phys.* **36**, 5431 (1995).

[51] N. Maroufi, V. Dehghani, S.A. Alavi, «Cluster Decay Half-life with Double-folding Potential: Uncertainty Analysis», *Acta Phys. Pol. B* **50**, 1349 (2019).

[52] T. Nikšić , N. Paar, D. Vretenar, P. Ring, «DIRHB — A relativistic self-consistent mean-field framework for atomic nuclei», *Comput. Phys. Commun.* **185**, 1808 (2014).

[53] J.T. Majekodunmi *et al.*, «Cluster decay half-lives of $^{112-122}$Ba isotopes from the ground state and intrinsic excited state using the relativistic mean-field formalism within the preformed-cluster-decay model», *Phys. Rev. C* **105**, 044617 (2022).

[54] P.G. Reinhard, «The relativistic mean-field description of nuclei and nuclear dynamics», *Rep. Prog. Phys.* **52**, 439 (1989).

[55] Y.K. Gambhir, P. Ring, A. Thimet, «Relativistic mean field theory for finite nuclei», *Ann. Phys.* **198**, 132 (1990).

[56] W.A. Yahya, B.I.S. Van Der Ventel, B.C. Kimene Kaya, R.A. Bark, «Calculation of a complete set of spin observables for proton elastic scattering from stable and unstable nuclei», *Phys. Rev. C* **98**, 014620 (2018).

[57] I. Ochala, J.O. Fiase, «B3Y-FETAL effective interaction in the folding analysis of elastic scattering of ^{16}O+^{16}O», *Nucl. Sci. Tech.* **32**, 81 (2021).

[58] W.A. Yahya, O.K. Azeez, J.T. Majekodunmi, G.D. Olawale, «Density-Dependent Parametrizations in B3Y-FETAL NN Interaction: Application to Alpha Decay», *Braz. J. Phys.* **54**, 74 (2024).

[59] W.A. Yahya *et al.*, «Effects of finite-range exchange terms and deformation on the α-decay half-lives using the B3Y NN interaction», *Phys. Rev. C* **111**, 024322 (2025).

[60] F. Ghorbani, S.A. Alavi, V. Dehghani, «Temperature dependence of the alpha decay half-lives of even–even Th isotopes», *Nucl. Phys. A* **1002**, 121947 (2020).

[61] B.D.C. Kimene Kaya, S.M. Wyngaardt, T.T. Ibrahim, W.A. Yahya, «Comparison of double-folding effective interactions within the cluster model», *Phys. Rev. C* **98**, 044308 (2018).

[62] D.N. Poenaru, W. Greiner, «Cluster preformation as barrier penetrability», *Phys. Scr.* **44**, 427 (1991).

[63] T.T. Ibrahim *et al.*, «Hybrid potential analysis of exotic clustering in heavy nuclei», *Phys. Rev. C* **85**, 044313 (2012).

[64] K.P. Santhosh, T.A. Jose, «Cluster decay half-lives using modified generalized liquid drop model (MGLDM) with different pre-formation factors», *Indian J. Phys.* **95**, 121 (2021).

[65] R. Blendowske, H. Walliser, «Systematics of Cluster-Radioactivity-Decay Constants as Suggested by Microscopic Calculations», *Phys. Rev. Lett.* **61**, 1930 (1988).

[66] K.P. Santhosh, V.K. Anjali, «Cluster radioactivity using modified generalized liquid model with a statistical cluster preformation probability», *Nucl. Phys. A* **1041**, 122787 (2024).

[67] L.J. Qi *et al.*, «Cluster radioactivity half-lives of trans-lead nuclei with a statistical physical preformation factor», *Eur. Phys. J. A* **59**, 255 (2023).

[68] I. Angeli, K.P. Marinova, «Table of experimental nuclear ground state charge radii: An update», *At. Data Nucl. Data Tables* **99**, 69 (2013).

[69] Y. Chu, Z. Ren, Z. Wang, T. Dong, «Central depression of nuclear charge density distribution», *Phys. Rev. C* **82**, 024320 (2010).

[70] A.V. Afanasjev, S. Frauendorf, «Central depression in nuclear density and its consequences for the shell structure of superheavy nuclei», *Phys. Rev. C* **71**, 024308 (2005).

[71] F.G. Kondev *et al.*, «The NUBASE2020 evaluation of nuclear physics properties», *Chinese Phys. C* **45**, 030001 (2021).

[72] K.P. Santhosh, V.K. Anjali, «Cluster radioactivity using modified generalized liquid model with a statistical cluster preformation probability», *Nucl. Phys. A* **1041**, 122787 (2024).

[73] G. Röpke, A. Schnell, P. Schuck, P. Nozières, «Four-Particle Condensate in Strongly Coupled Fermion Systems», *Phys. Rev. Lett.* **80**, 3177 (1998).

[74] R. Kumar, «Cluster radioactivity using various versions of nuclear proximity potentials», *Phys. Rev. C* **86**, 044612 (2012).

[75] N. Itagaki, A.V. Afanasjev, D. Ray, «Possibility of ^{14}C cluster as a building block of medium-mass nuclei», *Phys. Rev. C* **101**, 034304 (2020).

[76] K.P. Santhosh, T.A. Jose, «Half-lives of cluster radioactivity using the modified generalized liquid drop model with a new preformation factor», *Phys. Rev. C* **99**, 064604 (2019).